$Er^{3+}/Tm^{3+}/Yb^{3+}$ tridoped oxyfluoride glass ceramics with efficient upconversion white-light emission

Chenxia Li (李晨霞)[1,2], Shiqing Xu (徐时清)[2*], Renguang Ye (叶仁广)[2], Shilong Zhao (赵士龙)[2], Degang Deng (邓德刚)[2], and Songlin Zhuang (庄松林)[1]

[1]*School of Optical-Electrical and Computer Engineering, University of Shanghai for Science and Technology, Shanghai 200093, China*

[2]*College of Optical and Electronic Technology, China Jiliang University, Hangzhou 310018, China*

[*]*E-mail: sxucjlu@hotmail.com*

Received January 14, 2009

A novel $Tm^{3+}/Er^{3+}/Yb^{3+}$ triply-doped glass ceramics containing BaF_2 nano-crystals are successfully prepared. Fluoride nanocrystals BaF_2 are successfully precipitated in glass matrix, which is affirmed by the X-ray diffraction results. The intense blue (476 nm), green (543 nm), and red (656 nm) emissions of the glass ceramics are simultaneously observed at room temperature under 980-nm excitation, and the emission luminescence intensity increases significantly compared with the precursor glass, which is attributed to the low phonon energy of fluoride nanocrystals when rare-earth ions are incorporated into the precipitated BaF_2 nanocrystals. Under 980-nm excitation at 400 mW, the international commission on illumination (CIE) chromaticity coordinate ($X = 0.278$, $Y = 0.358$) of the tridoped oxyfluoride glass ceramics' upconversion emissions is close to the standard white-light illumination ($X = 0.333$, $Y = 0.333$). The results indicate that $Tm^{3+}/Er^{3+}/Yb^{3+}$ triply doped glass ceramics can act as suitable materials for potential three-dimensional displays applications.

OCIS codes: 160.4670, 160.5690.

doi: 10.3788/COL20100801.0066.

Recently, there has been an increasing interest in the upconversion of near infrared (NIR) light to visible light by rare earth (RE) ion doped materials due to the potential applications in areas such as three-dimensional (3D) display, optical data storage, optoelectronics, medical diagnostics, sensor, undersea optical communication, etc. For 3D displays based on the infrared to visible upconversion luminescence in rare earth doped materials, emission and control of the relative intensities of the three primary red, green, and blue (RGB) colors are required. Thus, there exists a need for novel solid-state materials capable of producing multicolor visible light. Indeed, there have been some reports on the control of luminescence in the three primary colors through upconversion and the generation of white light. For example, a 3D solid-state display was realized from fluoride glasses triply doped with Tm^{3+}, Er^{3+}, and Pr^{3+} using three different pairs of near-infrared laser excitation sources[1]. Despite the fact that the multiple-pump wavelength configurations can produce higher upconversion efficiencies, a single-pump scheme is mostly desired. The key technique to design upconversion luminescence materials was to situate the RE ions in low-phonon-energy environment. In the past few years, RGB upconversion emissions and white-light simulation were achieved in some RE-doped glasses under single infrared laser excitation[2−4]. However, the hosts were limited mainly in the fluoride and tellurite glasses. Oxyfluoride glass ceramics have been developed as ideal RE ion hosts used for upconversion devices since 1993. Such materials combined the low-phonon-energy environment of fluoride crystals and the high chemical and mechanical stability of oxide glasses[5−10]. Recently, Chen *et al*. reported white light emission in $Ho^{3+}/Tm^{3+}/Yb^{3+}$ triply-doped transparent glass ceramics through upconversion route[11]. However, there are no reports describing white light emission in $Er^{3+}/Tm^{3+}/Yb^{3+}$ triple-doped BaF_2 glass ceramics. In this letter, a novel $Er^{3+}/Tm^{3+}/Yb^{3+}$-doped oxyfluoride glass ceramics containing BaF_2 nanocrystals was successfully prepared and the bright white light with CIE-X 0.278 and CIE-Y 0.358 was generated through a single infrared laser source at 980 nm. The results indicate that they can act as suitable materials for potential 3D displays applications.

The glasses with composition of $52SiO_2$-$20Al_2O_3$-$13Na_2O$-5BaO-$10BaF_2$-$1Yb_2O_3$-$0.1Tm_2O_3$, $52SiO_2$-$20Al_2O_3$-$13Na_2O$-5BaO-$10BaF_2$-$1Yb_2O_3$-$0.1Er_2O_3$, and $52SiO_2$-$20Al_2O_3$-$13Na_2O$-5BaO-$10BaF_2$-$1Yb_2O_3$-$0.1Er_2O_3$-$0.1Tm_2O_3$(in mol-%) were prepared from high purity SiO_2, Al_2O_3, Na_2O, BaO, Yb_2O_3, Tm_2O_3, and Er_2O_3 raw materials named as G-A, G-B, and G-C. The mixed materials were melted in an alumina crucible at 1450 °C for about 40 min. The quenched sample was annealed at 300 °C for 2 h and cooled slowly to release the thermal stress associated with these glasses during the quenching process. The differential thermal analysis (DTA) result of the oxyfluoride glass shows that the transition temperature is 490 °C, and a weak crystallization peak occurs at 690 °C. According to the DTA curves the glass samples were heat-treated to 660 °C at a rate of 10 K/min, held for 2 h and then cooled to room temperature naturally to obtain the transparent glass ceramic named as GC-A, GC-B, and GC-C, respectively. X-ray diffraction (XRD) measurements were performed in a X'TRA diffractometer with Cu-K_α radiation at 4 °/min scanning rate. The

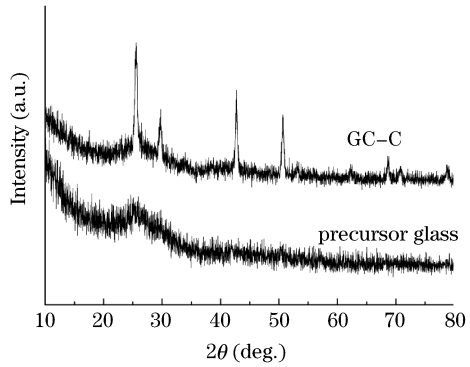

Fig. 1. XRD patterns of the parent glass GC and glass ceramics GC-C.

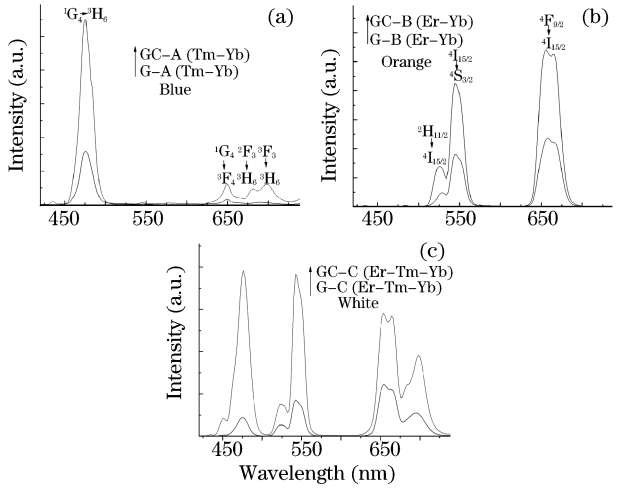

Fig. 2. Upconversion spectra from (a) G-A and GC-A samples, (b) G-B and GC-B samples, and (c) G-C and GC-C samples excited by a 980-nm LD of 400 mW.

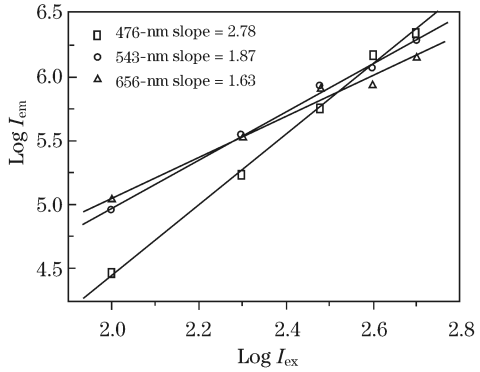

Fig. 3. Log-log plot of upconversion emission intensity as a function of the excitation power of GC-C sample.

emission luminescence spectra under excitation of 980-nm laser diode (LD) at 400 mW were measured with a Jobin-Yvon Frolog3 fluorescence spectrophotometer. In order to compare the luminescence intensity in different samples as accurate as we can, the position and width (1 mm) of the slit to collect the luminescence signals were set at the same place in the experimental setup. All the measurements were taken at room temperature.

The XRD patterns of the G-C and GC-C samples are presented in Fig. 1. The precursor glass G-C sample is completely amorphous without obvious diffraction peaks. After heat treatment, XRD patterns show intense diffraction peaks, which are easily assigned to the BaF_2crystal (JCPDS No. 85-1342). From the peak width of XRD pattern, the size of BaF_2 nanocrystals in the obtained glass ceramic is calculated to be about 23 nm by using Sherrer's equation: D=K$\lambda/\beta\cos\theta$. Here D is the crystal size at the vertical direction of (hkl), λ is the wavelength of X-ray, θ is the angle of diffraction, β is the full-width at half-maximum (FWHM) of the diffraction peak, and the constant K determined by β and the instrument. Due to the much smaller size of precipitated BaF_2 nanocrystals than wavelength of visible light, doped glass ceramics remain excellent transparency.

The upconversion luminescence spectra in the range from 420 to 740 nm of G-A, GC-A, G-B, GC-B, G-C, and GC-C under 980-nm excitation at 400 mW are shown in Fig. 2. The blue (476 nm) emission originated from the $^1G_4 \rightarrow {}^3H_6$ transition of Tm^{3+} was observed in the G-A and GC-A samples. In the G-B and GC-B samples green (522 and 543 nm) and red (656 nm) originated from $^2H_{11/2} \rightarrow {}^4I_{15/2}$, $^4S_{3/2} \rightarrow {}^4I_{15/2}$, and $^4F_{9/2} \rightarrow {}^4I_{15/2}$ transitions of Er^{3+}emissions were observed. Therefore by reasonable adjusting Tm^{3+}, Er^{3+}, and Yb^{3+} doping, the blue, green, and red emissions with the equal intensity were obtained in the $Tm^{3+}/Er^{3+}/Yb^{3+}$-tridoped glass ceramics GC-C sample, which yields the bright white light that can be clearly seen by naked eyes. Compared with the precursor glass, significant enhancement of luminescence was observed in the glass-ceramics. The reasons were as follows. Firstly, the doped ions should be incorporated into the fixed crystalline site positions. Structurally, glass is a continuous random network lacking both symmetry and periodicity. In the case of glasses the coordination of the rare earth ions becomes more delocalized[12]. As a consequence the oscillator strengths are also more dispersed. As shown in Fig. 1, BaF_2 crystal has formed after heat treatment. Therefore the emission luminescence intensity of the glass ceramics increases significantly. Secondly, intensity of luminescence is very sensitive to the multi-phonon relaxation rate of the rare-earth ions, which strongly depends on the phonon energy of the matrix. The larger the phonon energy and (or) the electron-phonon coupling strength, the larger the decay rate. That is to say, a decrease in the phonon energy and/or the electron-phonon coupling strength can increase the lifetime and quantum efficiency of excited levels, and consequently increase the emission intensity of the luminescence. The maximum phonon energy in silicate oxide glass is about 1100 cm^{-1}. However, the maximum phonon energy of BaF_2 is 346 cm^{-1}[13], which is significantly lower than that in glass matrix. The above two reasons lead to a decrease in the non-radiative decay rate. Thus compared with the precursor glass, the emission intensity of the glass ceramics enhances.

In the upconversion processes, there is a following relation between the upconversion emission intensity I_{em} and the infrared (IR) excitation intensity I_{ex}: $I_{em} \propto (I_{ex})^n$[14,15], where n is the number of IR photons absorbed per visible photon emitted. Therefore, a plot of $\log(I_{em})$ versus $\log(I_{ex})$ of the GC-C sample should yield a straight line with the slope n, as shown in Fig. 3. The slopes of 476, 543, and 656 nm emission are 2.78, 1.87, and 1.63, respectively. The results indicate that the blue

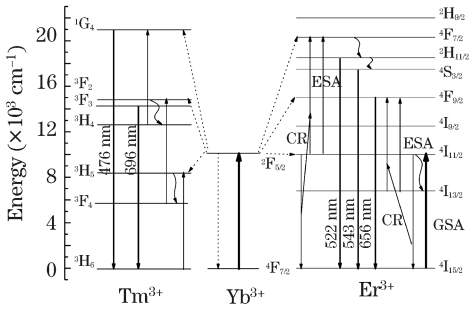

Fig. 4. Simple energy level diagram of Tm^{3+}, Er^{3+}, and Yb^{3+} ions and the possible upconversion mechanism.

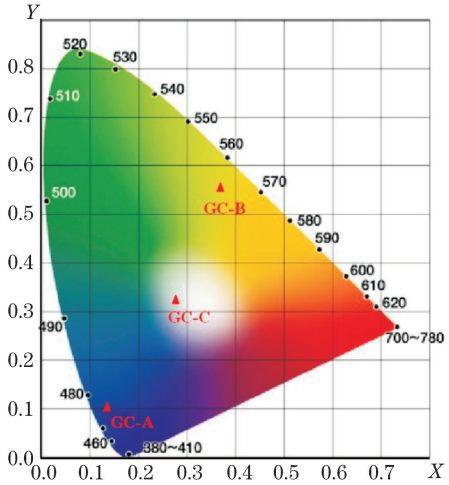

Fig. 5. CIE (X, Y) coordinate diagram that shows the chromaticity points of the emissions in the samples excited by 980 nm at 400 mW.

emission can be described as a three-photon mechanism, and the green and red emission can be described as a two-photon mechanism. The reason that the slopes of 543- and 656-nm emssion are smaller than 2 is mainly a saturation effect because the pump beam is focused into the sample. An increased slope value of 2 can be obtained when the laser beam is defocused. Similar effects due to saturation have been observed and discussed[16].

According to the energy matching conditions, the possible upconversion for the blue, green, and red emissions mechanism of $Tm^{3+}/Er^{3+}/Yb^{3+}$ ions of the GC-C sample is proposed, as depicted in Fig. 4. The blue emission of 476-nm process for the $^1G_4 \rightarrow {}^3H_6$ transition and the red emission of 696-nm process for the $^3H_3 \rightarrow {}^3H_6$ transition of Tm^{3+} can be explained as follows. In the first step, a 980-nm photon is absorbed by Yb^{3+}, which provokes the $^2F_{7/2} \rightarrow {}^2F_{5/2}$ transition, and then the excitation of Tm^{3+} in the $^3H_5$ is involved by means of the energy transfer (ET) mechanism of excited Yb^{3+} to Tm^{3+}: ET: $^2F_{5/2}(Yb^{3+}) + {}^3H_6(Tm^{3+}) \rightarrow {}^2F_{7/2}(Yb^{3+}) + {}^3H_5(Tm^{3+})$. In the second step, Tm^{3+} in the $^3H_5$ excited state relaxes nonradiatively to the meta-state level. Tm^{3+} in the $^3F_4$ level is excited to $^3F_{2,3}$ level by ET from Yb^{3+} and absorbs one photon. Thus the population of $^3F_{2,3}$ is based on the processes as follows: ET from Yb^{3+}: $^2F_{5/2}(Yb^{3+}) + {}^3F_4(Tm^{3+}) \rightarrow {}^2F_{7/2}(Yb^{3+}) + {}^3F_{2,3}(Tm^{3+})$, and excited state absorption: $^3F_4(Tm^{3+})$ + one photon $\rightarrow {}^3F_{2,3}(Tm^{3+})$. From the $^3F_3$ level, the Tm^{3+} ions decay radiatively to the $^3H_6$ ground state generating the red emission around 696 nm. Then the Tm^{3+} in $^3F_{2,3}$ state also relaxes by a multiphonon assisted process to the $^3H_4$ level. Finally, Tm^{3+} in the $^3H_4$ level is excited to $^1G_4$ level by ET from Yb^{3+} and absorbs one photon. Therefore, the population of $^1G_4$ is based on the processes as follows: ET from Yb^{3+}: $^2F_{5/2}(Yb^{3+}) + {}^3H_4(Tm^{3+}) \rightarrow {}^2F_{7/2}(Yb^{3+}) + {}^1G_4(Tm^{3+})$, and excited state absorption: $^3H_4(Tm^{3+})$ + one photon $\rightarrow {}^1G_4(Tm^{3+})$. From the above results it can be concluded that a two-phonon absorption process is responsible for red (696 nm) emission and a three-phonon absorption process is responsible for blue (476 nm) emission. The green (522 and 543 nm) and red (656 nm) excitation processes are for the $^2H_{11/2} \rightarrow {}^4I_{15/2}$, $^4S_{3/2} \rightarrow {}^4I_{15/2}$, and $^4F_{9/2} \rightarrow {}^4I_{15/2}$ transitions of Er^{3+}, respectively. In the first step, the $^4I_{11/2}$ level is directly excited with 980 nm light by ground state absorption (GSA) and/or by ET process from $^2F_{5/2}$ level of Yb^{3+}: $^2F_{5/2}(Yb^{3+}) + {}^4I_{15/2}(Er^{3+}) \rightarrow {}^4I_{11/2}(Er^{3+}) + {}^2F_{7/2}(Yb^{3+})$. The second step involves the excitation processes based on the long-lived $^4I_{11/2}$ level as follows: cross-relaxation (CR): $^4I_{11/2}(Er^{3+}) + {}^4I_{11/2}(Er^{3+}) \rightarrow {}^4F_{7/2}(Er^{3+}) + {}^4I_{15/2}(Er^{3+})$, excited state absorption (ESA): $^4I_{11/2}(Er^{3+})$ + one photon $\rightarrow {}^4F_{7/2}(Er^{3+})$, and ET: $^2F_{5/2}(Yb^{3+}) + {}^4I_{11/2}(Er^{3+}) \rightarrow {}^2F_{7/2}(Yb^{3+}) + {}^4F_{7/2}(Er^{3+})$. The populated $^4F_{7/2}$ level of Er^{3+} then relaxes rapidly and nonradiatively to the next lower levels $^2H_{11/2}$ and $^4S_{3/2}$ resulting from the small energy gap between them. The above processes then produce the two $^2H_{11/2} \rightarrow {}^4I_{15/2}$ and $^4S_{3/2} \rightarrow {}^4I_{15/2}$ green emissions centered at 522 and 543 nm, respectively. The red emission entered at 656 nm is originated from the $^4F_{9/2} \rightarrow {}^4I_{15/2}$ transition. The population of $^4F_{9/2}$ are based on the processes as follows: ESA: $^4I_{13/2}(Er^{3+})$ + one photon $\rightarrow {}^4F_{9/2}(Er^{3+})$, CR between Er^{3+} ions: $^4I_{13/2}(Er^{3+}) + {}^4I_{11/2}(Er^{3+}) \rightarrow {}^4I_{15/2}(Er^{3+}) + {}^4F_{9/2}(Er^{3+})$, and ET from Yb^{3+}: $^2F_{5/2}(Yb^{3+}) + {}^4I_{13/2}(Er^{3+}) \rightarrow {}^2F_{7/2}(Yb^{3+}) + {}^4F_{9/2}(Er^{3+})$. The $^4I_{13/2}$ level is populated owing to the nonradiative relaxation from the upper $^4I_{11/2}$ level. Besides, the nonradiative process from $^4S_{3/2}$ level, which is populated by means of the process described previously, to $^4F_{9/2}$ level, also contributes to the red emission. From the above results it can be concluded that a two-phonon upconversion process is responsible for green (522 and 543 nm) and red (656 nm) emissions.

The upconversion emission spectra for the samples pumped by 980 nm at 400 mW are converted to the CIE 1931 chromaticity diagram and plotted in Fig. 5. For the samples of GC-A (Tm^{3+}/Yb^{3+}-doped glass ceramic) and GC-B (Er^{3+}/Yb^{3+}-doped glass ceramic), blue emissions with CIE coordinate ($X = 0.137$, $Y = 0.114$) and orange emissions with CIE coordinate ($X = 0.370$, $Y = 0.614$) are achieved, respectively. While for the GC-C sample ($Tm^{3+}/Er^{3+}/Yb^{3+}$ triply doped glass ceramic), the luminescence is tuned to white. Apparently its CIE coordinate ($X = 0.278$, $Y = 0.358$) in Fig. 5 is close to the standard equal energy white-light illumination ($X = 0.333$, $Y = 0.333$).

In conclusion, a novel $Tm^{3+}/Er^{3+}/Yb^{3+}$ triply doped glass ceramic containing BF_2 nano-crystals were successfully prepared. Bright white light with CIE-X 0.278 and CIE-Y 0.358 was generated through frequency excited by a single infrared laser diode source at 980 nm. Intense upconversion luminescence emissions around 476, 543, and 656 nm were recorded. The 476-nm blue signal was attributed to Tm^{3+} excited by a three-phonon absorption process. The green (543 nm) and red (656 nm) upconversion luminescence were identified mainly from the Er^{3+} excited by a two-phonon absorption process. The results indicate that $Tm^{3+}/Er^{3+}/Yb^{3+}$-codoped glass can be used as host material for potential 3D display applications.

This work was supported by the National Natural Science Foundation of China (Nos. 60508014 and 50772102), the Program for New Century Excellent Talents in University (No. NCET-07-0786), the Science Technology Project of Zhejiang Province (No. 2008C21162), and the Natural Science Foundation of Zhejiang Province (No. R406007).

References

1. E. Downing, L. Hesselink, J. Ralston, and R. Macfarlane, Science **273,** 1185 (1996).
2. J. E. C. da Silva, G. F. de Sá, and P. A. Santa-Cruz, J. Alloys Compd. **344,** 260 (2002).
3. S. Xu, H. Ma, D. Fang, Z. Zhang, and Z. Jiang, Mater. Lett. **59,** 3066 (2005).
4. H. T. Amorim, M. V. D. Vermelho, A. S. Gouveia-Neto, F. C. Cassanjes, S. J. L. Ribeiro, and Y. Messaddeq, J. Solid State Chem. **171,** 278 (2003).
5. M. Liao, L. Hu, Y. Fang, J. Zhang, H. Sun, S. Xu, and L. Zhang, Spectrochim. Acta Part A **68,** 531 (2007).
6. D. Chen, Y. Wang, K. Zheng, T. Guo, Y. Yu, and P. Huang, Appl. Phys. Lett. **91,** 251903 (2007).
7. A. S. Gouveia-Neto, L. A. Bueno, R. F. do Nascimento, E. A. da Silva, Jr., E. B. da Costa, and V. B. do Nascimento, Appl. Phys. Lett. **91,** 091114 (2007).
8. F. Liu, E. Ma, D. Chen, Y. Yu, and Y. Wang, J. Phys. Chem. B **110,** 20843 (2006).
9. H. Yu, L. Zhao, J. Meng, Q. Liang, X. Yu, B. Tang, and J. Xu, Chin. Opt. Lett. **3,** 469 (2005).
10. M. Beggiora, I. M. Reaney, A. B. Seddon, D. Furniss, S. A. Tikhomirova, J. Non-Cryst. Solids **326&327,** 476 (2003).
11. D. Chen, Y. Wang, Y. Yu, P. Huang, and F. Weng, J. Solid State Chem. **181,** 2763 (2008).
12. G. Lakshminarayana, H. Yang, Y. Teng, and J. Qiu, J. Lumin. **129,** 59 (2009).
13. S. A. Pollack and D. B. Chang, J. Appl. Phys. **64,** 2885 (1988).
14. Y. Zhou, J. Wang, S. Dai, X. Shen, T. Xu, and Q. Nie, Chinese J. Lasers (in Chinese) **34,** 1688 (2007).
15. S. Zhao, F. Zheng, S. Xu, H. Wang, and B. Wang, Chin. Opt. Lett. **6,** 276 (2008).
16. Z. Pan, S. H. Morgan, A. Loper, V. King, B. H. Long, and W. E. Collins. J. Appl. Phys. **77,** 4688 (1995).